Title

Bioorthogonal Stimulated Raman Scattering Imaging Uncovers Lipid Metabolic Dynamics in Drosophila Brain During Aging

Journal

GEN Biotechnology, 2(3)

ISSN

2768-1556

Authors

Li, Yajuan

Chang, Phyllis

Sankaran, Shriya

et al.

Publication Date

2023-06-01

DOI

10.1089/genbio.2023.0017

Peer reviewed

GEN Biotechnology
Volume 2, Number 3, 2023

DOI: 10.1089/genbio.2023.0017

GEN Biotechnology

RESEARCH ARTICLE

Bioorthogonal Stimulated Raman Scattering Imaging Uncovers Lipid Metabolic Dynamics in *Drosophila* Brain During Aging

Yajuan Li,[1] Phyllis Chang,[1] Shriya Sankaran,[1] Hongje Jang,[1] Yuhang Nie,[2] Audrey Zeng,[1] Sahran Hussain,[1] Jane Y. Wu,[3] Xu Chen,[2] and Lingyan Shi[1,*]

Abstract

Studies have shown that brain lipid metabolism is associated with biological aging and influenced by dietary and genetic manipulations; however, the underlying mechanisms are elusive. High-resolution imaging techniques propose a novel and potent approach to understanding lipid metabolic dynamics *in situ*. Applying deuterium water (D_2O) probing with stimulated Raman scattering (DO-SRS) microscopy, we revealed that lipid metabolic activity in *Drosophila* brain decreased with aging in a sex-dependent manner. Female flies showed an earlier occurrence of lipid turnover decrease than males. Dietary restriction (DR) and downregulation of insulin/IGF-1 signaling (IIS) pathway, two scenarios for lifespan extension, led to significant enhancements of brain lipid turnover in old flies. Combining SRS imaging with deuterated bioorthogonal probes (deuterated glucose and deuterated acetate), we discovered that, under DR treatment and downregulation of IIS pathway, brain metabolism shifted to use acetate as a major carbon source for lipid synthesis. For the first time, our study directly visualizes and quantifies spatiotemporal alterations of lipid turnover in *Drosophila* brain at the single organelle (lipid droplet) level. Our study not only demonstrates a new approach for studying brain lipid metabolic activity *in situ* but also illuminates the interconnection of aging, dietary, and genetic manipulations on brain lipid metabolic regulation.

Aging is an almost universal phenomenon for living organisms and is associated with progressive deterioration of physiological functions and increased susceptibility to diseases and death.[1] Lipid metabolism has been associated with aging and age-related diseases.[2] The brain is a lipid-enriched organ, second only to the adipose tissue.[3] Previous studies reported a decline of omega-3 fatty acids and an increase in lipid peroxidation in aged brains.[4,5] Dietary deficiency of omega-3 fatty acids may accelerate neurodegeneration,[6,7] indicating the critical role of lipid metabolism in brain function. Genome-wide association study (GWAS) suggests that lipid metabolism changes in the brain may have impact on aging and longevity.[8]

One group of brain lipids include sphingolipids, glycerophospholipids, and cholesterol, which serve as critical building materials for cell and organelle membranes, and are involved in cell signal transduction.[9] Another group of lipids that play nonstructural roles in the brain are triacylglycerol (TAGs) and steryl esters, which are wrapped in lipid droplets (LDs) for energy storage. Electron microscopy study demonstrated that LDs in the nervous system are mainly localized in glial cells.[10–12] Many studies revealed valuable insights into the role of LDs play in aging and neurodegeneration. For example, reactive oxygen species (ROS) induced by mitochondrial dysfunction increase the activities of c-Jun-N-terminal Kinase and sterol regulatory element binding protein, leading to the accumulation of LDs in glial cells before or at the onset of neuronal loss.

LD accumulation in glial cells promotes neurodegeneration and represents as an early transient indicator of neuronal death.[13] LDs in glial cells can also protect polyunsaturated fatty acids in brain membranes from oxidation to maintain the proliferation of *Drosophila* neural stem cells under oxidative stress.[14] The accumulation of LDs in microglia has been reported involved in age-related and genetic forms of neurodegeneration.[12] These lipid-droplet-accumulating microglia, characterized as pathological glial cells, are defective in phagocytosis, produce high levels of ROS and secrete proinflammatory cytokines. The inability to transport lipids to glia for LD formation leads to accelerated neurodegeneration under stress.[15]

Despite these efforts, how brain lipid metabolism is dynamically modulated by the aging process has not been fully understood. Alterations in nutrition balance is a notable cause of aging,[16–18] but how diets and metabolic pathways regulate

[1]*Department of Bioengineering, University of California San Diego, La Jolla, California, USA;* [2]*Department of Neurosciences, School of Medicine, University of California San Diego, La Jolla, California, USA; and* [3]*Department of Neurology, Feinberg School of Medicine, Northwestern University, Chicago, Illinois, USA.*

*Address correspondence to: *Lingyan Shi, Department of Bioengineering, University of California San Diego, La Jolla, CA 92093, USA,* E-mail: lingyanshi@ucsd.edu

brain lipid metabolism remain elusive. One major reason for this is the lack of high-resolution imaging method to track brain metabolic activity *in situ*. Stimulated Raman scattering (SRS) imaging combined with deuterium water (D_2O; DO-SRS) has been used to investigate the metabolic activity in *Drosophila* fat body.[19,20]

In this study, integrated with other bioorthogonal probes, for example, deuterated glucose and acetate, we used DO-SRS to investigate brain lipid metabolism at an even small single organelle level (1–2 μm LD) in *Drosophila* normal aging and longevity models. We discovered that the lipid metabolic dynamics and pathways are influenced and modulated by sex, diet, and insulin/IGF-1 signaling (IIS) pathway manipulation. These findings will project insights into mechanisms underlying age-related neurodegenerative diseases.

Results

Label-free SRS imaging visualized dynamic changes of lipid metabolism in *Drosophila* aging brain

As one of the classic aging model organisms, *Drosophila* has a short lifespan, shares ~60% genes with humans (including about 75% of those linked to human diseases), and offers powerful genetic and molecular tools to finely dissect the gene functions and physiology.[21] *Drosophila* brain with its relatively small and simple structure but functionally analogous to mammals has the main advantage to be metabolically analyzed as one whole intact tissue. *Drosophila* brain can be roughly divided into two compartments: the central brain (CB) and the optic lobe (OL). Each compartment is subdivided into anatomically discrete cortex and neuropil regions (Fig. 1A).

Based on its chemical selectivity, SRS can be used to visualize the subcellular localization of different types of molecules in cells and tissues without any labeling. To investigate the metabolic changes of *Drosophila* brain, we first used label-free SRS imaging and Raman spectroscopy to detect and track the endogenous lipids and proteins of the whole-mount brain during *Drosophila* aging process. The Raman spectra we collected displayed a dramatic reduction of the peak intensity at 2850 cm^{-1} (CH_2 from lipids) in 35-day-old brains (Fig. 1B, E and Supplementary Fig. S1A).[22] Consistently, SRS imaging showed the global lipid signal (green channel at 2850 cm^{-1}) was markedly weak in both the CBs and OLs of aged brains (Fig. 1C, D and Supplementary Fig. S1C, D).

This lipid reduction phenotype is consistent with that found in aged mice and human.[12,23,24] In addition, the normalized abundance of unsaturated lipids (peak at 1656 cm^{-1}) also showed a significant reduction in the aged brains (Fig. 1F and Supplementary Fig. S1A, B). Of note, stimulated Raman histology (SRH) images were generated from protein (2930 cm^{-1}) and lipid (2850 cm^{-1}) SRS channels, which mimicked histological hematoxylin and eosin staining.[25] SRH images clearly displayed structural changes in old *Drosophila* brains. Compared with young brains, old brains demonstrate increased vacuoles-like structures, shape alterations, and blurred boundaries in the neuropils (the highly dense compartments of CBs: mushroom bodies and antennal lobes; Fig. 1C, D and Supplementary Fig. S1C, D).

We noticed the lipid signal was dominantly located in the dot-like structures in the brain cortex regions (Fig. 1C, D and Supplementary Fig. S1C, D), which reminded us of brain LDs.[10,12–14] We thus co-registered BODIPY staining with SRS imaging and verified these lipid signals were mainly from LDs (Supplementary Fig. S1E). The 3D high-resolved SRS imaging showed that these LDs were 1–2 μm in diameter and mainly localized on the surface of brain cortex (Supplementary Fig. S1F, G).[26] We then imaged and quantified the changes of brain LD density and size during aging in these regions (Fig. 1G–I). We found the LD density was decreased whereas the size was increased with aging in both females and males. Intriguingly, the LD density was consistently higher and LD size was increased more in females during aging than those in males. It indicates that brain lipid metabolism was altered in an age- and sex-dependent manner.

SRS imaging revealed LDs mainly localized in the glia of adult brain

LDs are dynamic organelles with heterogeneous size and location according to various contexts.[27] Previous studies showed that LDs in *Drosophila* larval and mouse brains were mainly localized in glia and consisted of TAGs.[12,14] To examine the subcellular distribution of LDs in *Drosophila* brain, we used glia-specific Gal4-driven GFP to coregister with the SRS detected LDs, and found they were colocalized (Fig. 2A).

To illuminate the constitution of brain LDs, we manipulated the expressions of three key enzymes in TAG synthesis and mobilization specifically in glia, including Lipin (3-sn-phosphatidate phosphohydrolase), diacylglycerol acyltransferase 1 (DGAT1), and brummer (bmm, the fly homologue of adipose triglyceride lipase [ATGL]). We found that the brain LD density was significantly reduced in flies with Lipin or DGAT1 knockdown, or bmm overexpression (Fig. 2B, C), verifying that TAGs were the main contents of LDs, and further confirming these LDs were dominantly localized in glia.

The lipid contents inside LDs can vary greatly between cell types or even same type under different (age) contexts.[27] Any changes of LD content could be sensitively delineated by the shape changes of Raman spectra.[28] We, therefore, conducted SRS hyperspectral imaging (SRS-HSI) of single brain LD and compared LD contents in *Drosophila* at different ages and sexes (Supplementary Fig. S2). Dominant Raman peaks were found at 2850, 2880, 2930, and 3009 cm^{-1}, respectively, which were consistent with those peaks in the spontaneous Raman spectra collected from a small volume (several μm^3) of the whole brain tissues (Figs. 1B and 2D; Supplementary Fig. S1A).

SRS-HSI collects signal from individual pixel, which prevents the extraction of LD signal from neighboring cellular structures. LD spectra derived from SRS-HSI show no significant differences between young and aged brains, except for a slightly higher peak intensity at 2850 cm^{-1} in old brains, correspondingly, a slightly higher lipid to protein ratio (Fig. 2D). This is consistent with the larger LD size we previously observed in the old brains—since protein abundance is associated with LD surface area, it reduces when LD grows larger (reduced surface area to volume ratio), which leads to a higher lipid to protein ratio.

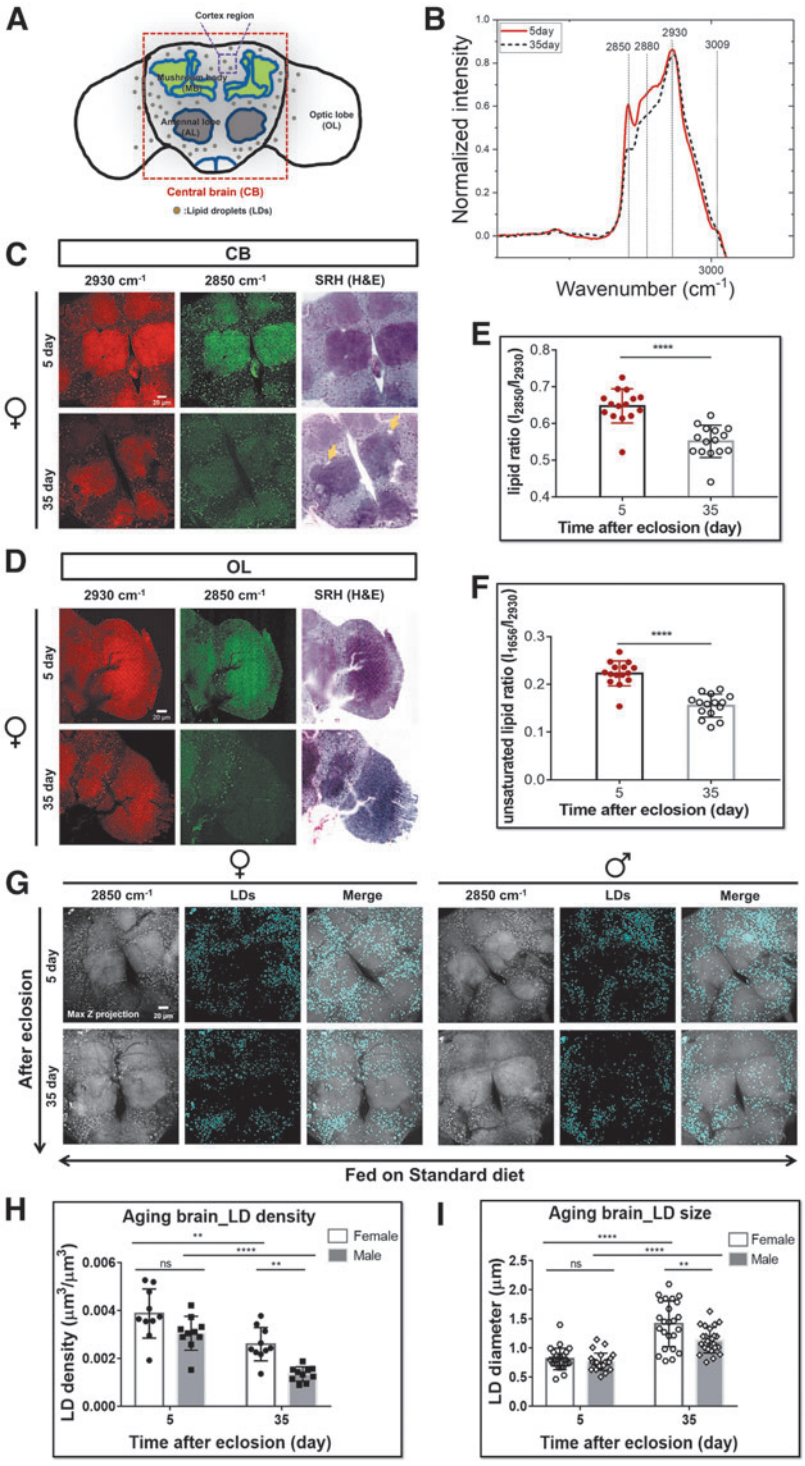

FIG. 1. Lipid metabolic changes in *Drosophila* brain detected by Raman and SRS microscopy.

(A) A cartoon of *Drosophila* adult brain depicting the structures of CB and optic lobe (OL). In the CB, the highly dense compartments of CBs (MBs and ALs) represent the neuropils, whereas the cortex takes up the rest of brain. The gray dots are representative of LDs.

(B) Raman spectra of brains from 5- and 35-day-old flies. The peaks at 2850, 2880, 2930, and 3009 cm^{-1} correspond to lipids, asymmetric CH_2 stretching bond of lipids, proteins, and unsaturated lipids, respectively.

(C, D) SRS imaging of the CB **(C)** and optic lobe **(D)** regions from 5- and 35-day flies. Distributions of proteins and lipids were visualized at 2930 and 2850 cm^{-1}, respectively. SRH images were generated from protein and lipid channels. The orange arrows show the vacuoles in old brains. Scale bar: 20 μm.

(E, F) Quantification of the ratios of total lipids (2850 cm^{-1}) **(E)** and unsaturated lipids (1656 cm^{-1}) **(F)** to proteins (2930 cm^{-1}). Data are presented as mean ± SD. $n = 15$ for each age group.

(G) Max Z projection of 3D brain images from females and males at different ages were displayed to show LD distribution. Scale bar: 20 μm.

(H, I) Quantitative comparison of LD density (total LD volume to brain cortex volume) **(H)** and diameter **(I)** in female and male brains at different ages (5- and 35-day). Results were presented as mean ± SD and compared. $n = 8$–10 brains (from at least three technical repeats) for each age group. Statistical significance was determined by Student's *t*-test **(E, F)** or one-way ANOVA **(H, I)**. $^{**}p < 0.01$; $^{****}p < 0.0001$; ns, nonsignificant difference. ANOVA, analysis of variance; CB, central brain; LD, lipid droplet; OL, optic lobe; MB, mushroom body; AL, antennal lobe; SD, standard deviation; SRH, stimulated Raman histology; SRS, stimulated Raman scattering imaging. For readability, please view the figure online.

DO-SRS imaging revealed brain lipid metabolic activity gradually decreased with aging

Remodeling of LD size is regulated by lipogenesis and lipolysis.[29,30] To understand the mechanism underlying dynamic changes of brain LDs, we examined the lipid metabolic activity at single LD level during fly aging by using DO-SRS imaging.[19] Once entering the body, D_2O will be incorporated into brain lipid metabolism, and the deuterium (D)-labeled lipids in LDs can be detected by SRS *in situ*. After feeding flies at different ages (0, 10, 20, 30, and 40 days posteclosion) with diets containing 20% D_2O for 5 days (Supplementary Fig. S3A), we imaged brain LDs and quantified lipid turnover by the ratio of CD signal (newly synthesized lipids) to CH signal (total lipids) collected at 2143 and 2850 cm^{-1}, respectively.[19,20]

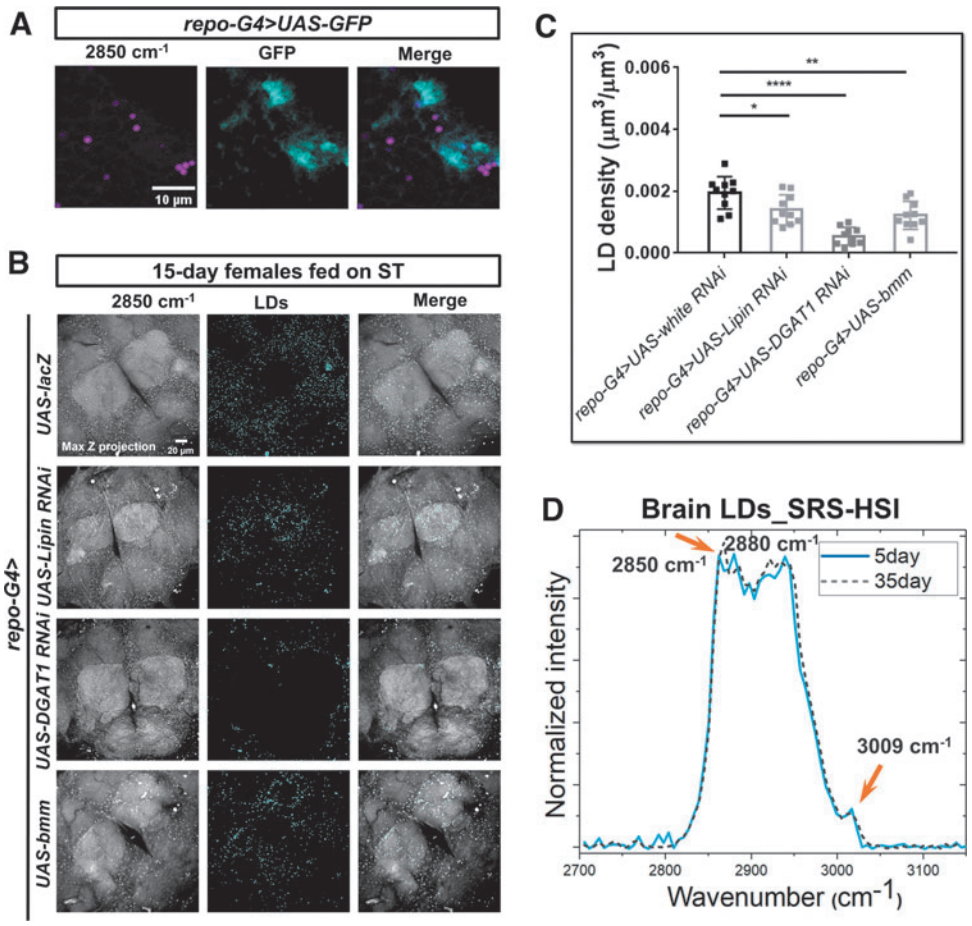

FIG. 2. TAGs are the predominant constituent of glial LDs.

(A) SRS detected LD signal (magenta) colocalized with glial cells (cyan).

(B) Max Z projected SRS images of brain from flies with glial-specific gene knockdowns (*repo-G4>UAS-RNAi*) of TAG synthetic enzymes (*Lipin*, or *DGAT1*) or overexpression of TAG lipase (*bmm*) were compared with the control group (*repo-G4>UAS-lacZ*). Scale bar: 20 μm.

(C) LD density in **(B)** was quantified and presented as mean ± SD ($n = 5$–8 brains, from at least three technical repeats).

(D) The SRS-hyperspectral imaging (HSI) spectra were taken from 5- and 35-day-old female brain LDs, and the spectra of CH regions were plotted. Total lipids peak (2850 cm^{-1}) and unsaturated lipids peak (3009 cm^{-1}) were marked by the orange arrows. Statistical significance was determined by using one-way ANOVA. *$p < 0.05$; **$p < 0.01$; ****$p < 0.0001$; ns, nonsignificant difference; HSI, hyperspectral imaging; TAG, triacylglycerol.

DO-SRS imaging revealed strong time-dependent deuterium incorporation from D_2O-containing dietary water into LDs (Fig. 3A and Supplementary Fig. S3B), suggesting that *de novo* lipogenesis contributes neutral lipid cargo to LDs. DO-SRS images also showed nonuniform distribution of newly synthesized lipids inside individual LDs (Fig. 3A), which is consistent with those observed in *Drosophila* fat body.[20]

Quantification results displayed the same trend of lipid turnover rate (CD/CH ratio) changing with aging in both female and male flies (Fig. 3B, C). It gradually increased in young flies (5–15 days), to a maximum in mid-aged (15–35 days), and then declined in aged flies (35–45 days). Nevertheless, lipid turnover also displayed sexual differences during aging (Supplementary Table S2). It reached a maximum at an earlier stage in female flies than in males (25 days vs. 35 days), and the turnover rates were consistently higher in young and mid-aged females but lower in 45-day ones. Together, these indicate earlier and more active lipid metabolism in females, whereas males have the opposite trend during aging. It again verified the sex dimorphism in brain metabolism.

LD is a highly dynamic organelle, the inside lipid turnover rate measured was the result of the balance between lipogenesis and lipolysis. That is, the deuterium-labeled lipids (CD signal) observed were the net newly synthesized lipids. We measured lipid turnover decreased during aging, whereas LD size was enlarged in aged brains (Fig. 1G–I), suggesting that lipolysis in LDs was compromised. To test this hypothesis, we utilized a starvation assay that facilitated the mobilization of stored lipids. We treated 0-day (young) and 30-day (aged) flies with standard diet containing 20% D_2O for 10 days to obtain saturated deuterium

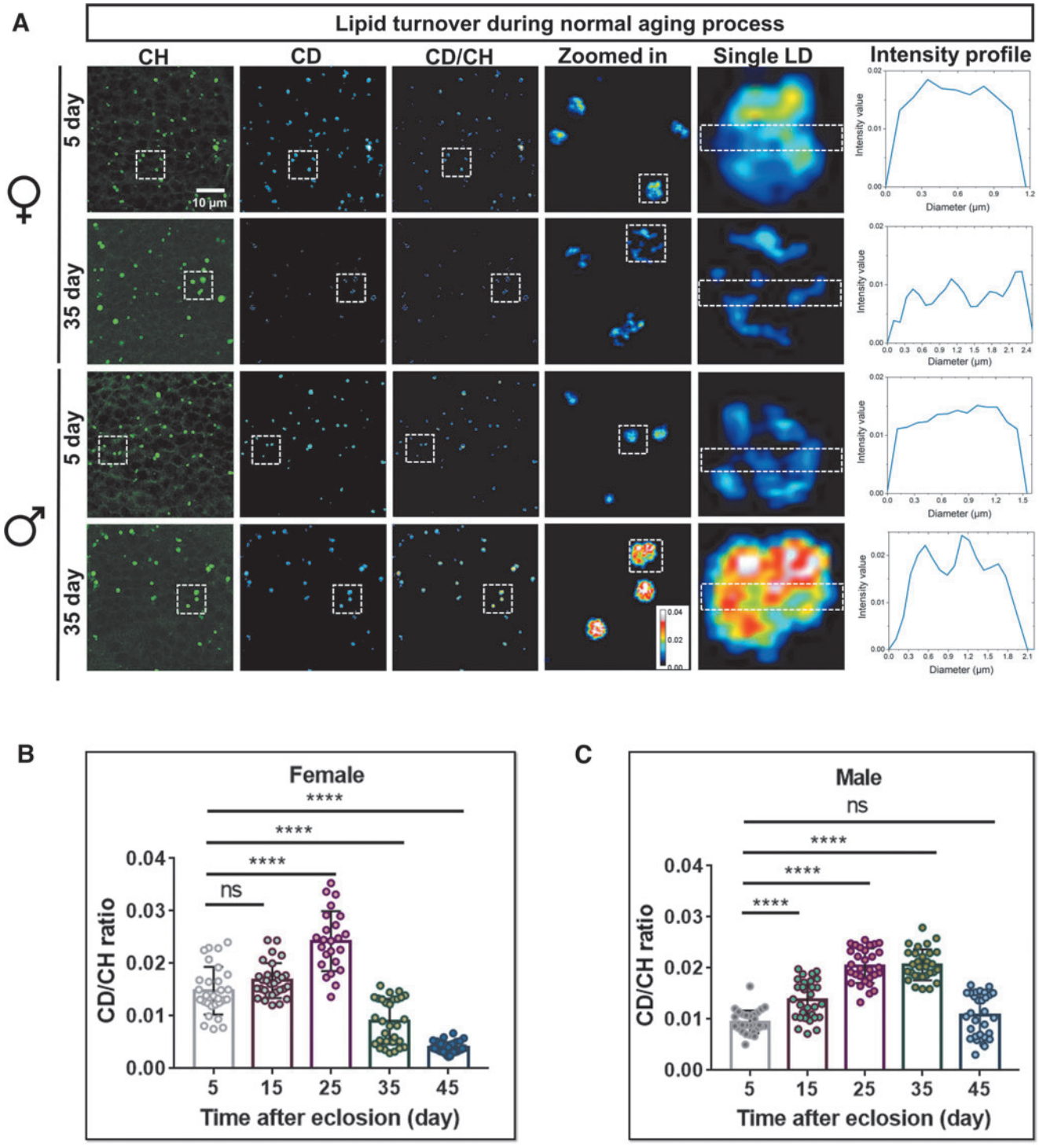

FIG. 3. Visualizing the metabolic activities of brain LDs during aging by DO-SRS imaging.

(A) DO-SRS imaging of brain LDs in 5- and 35-day female and male flies. Images were taken at 2850 and 2143 cm^{-1}, respectively. The signals were color-coded in green (CH, total lipids), cyan (CD, newly synthesized lipids), and royal (CD/CH), respectively. The representative LDs inside the dashed boxes were magnified. The intensity profiles inside individual LDs were plotted to show the distribution of newly synthesized lipids. Scale bar: 10 μm.

(B, C) Quantification of CD/CH ratios in brain LDs from female **(B)** and male **(C)** flies. Flies at 0-, 10-, 20-, 30-, and 40-day old were fed with 20% D_2O-containing standard diet (ST) for 5 days. Brain LDs were then imaged at 2143 cm^{-1} (CD, newly synthesized lipids) and 2850 cm^{-1} (CH, total lipids), respectively, and the ratios of newly synthesized lipids to total lipids (CD/CH) (lipid turnover) were quantified. Data are presented as mean ± SD. $n = 30$ ROIs from 8 brains, 3 technical repeats. Statistical significance was determined by using one-way ANOVA. ****$p < 0.0001$; ns, nonsignificant difference. D_2O, deuterium water; DO-SRS, deuterium water probed stimulated Raman scattering; ROIs, regions of interest; ST, standard diet.

incorporation (~2.7%) for DO-SRS imaging (Supplementary Fig. S3B), and then transferred the flies to 1% agar for starvation.

The CD/CH ratios in brain LDs were examined at 24, 48, and 72 h of the starvation, respectively (Supplementary Fig. S3C, D). The CD-chasing curves indicate that lipid turnover decreased faster in young flies than aged ones in both sexes, and faster in old males than in old females. The latter indicates old male flies had a higher lipolytic rate than age-matched females (52% vs. 76% of initial CD/CH ratio after 72 h starvation), that is, male mobilized more lipids than female. Data together indicated that, compared with young brains, old brains have inert lipid turnover. The dramatic decline of lipolysis in single LD of old flies may lead to the enlarged LD size. These data together indicate brain lipid metabolism is highly dynamic, especially at the young stages, and DO-SRS provides the sufficient sensitivity in the quantification of lipid turnover.

DO-SRS imaging illuminated brain lipid turnover significantly increased under dietary restriction

Dietary restriction (DR) has been considered an efficient approach to promote motor ability and extend healthy lifespan.[31–34] Interestingly, DR benefits females' lifespan more than males' lifespan.[35] To investigate how DR modulates brain lipid metabolism in different sexes, we imaged and quantified brain lipid turnover rate in both female and male flies at different ages under DR (Fig. 4A, B). Similar to that in the normal aging process, the lipid turnover rate under DR increased first and then declined along aging.

However, DR remarkably enhanced brain lipid turnover in 45-day old animals in both sexes, to a higher extent in females (3.6- and 2.1-fold in female and male, respectively) (Fig. 4B and Supplementary Table S3). That is, DR prevented LD metabolic activity from becoming inert with aging (Fig. 4G). We also detected average LD size was reduced under DR treatment, but no significant changes in LD density (Fig. 4C, D).

We next investigated if the lipid metabolic activity was correlated with brain function. By using the negative geotaxis climbing assay, we were able to assess the locomotor activity, which can partially reflect brain neuronal functions.[36] Consistent with previous studies, we observed an age-dependent decline of locomotor function with normal aging (Fig. 4E). DR decelerated the decline rate of motor function in both females and males (Fig. 4E and Supplementary Table S4). The correlation analysis further verified the association of locomotor function with LD lipid turnover rate in old females understandard diet (ST) and DR treatments (Fig. 4F). We thus concluded that DR might modulate the brain function through regulating brain lipid metabolism.

DO-SRS imaging illustrated reducing IIS activity upregulated lipid turnover

The IIS pathway is a critical regulator of development and aging that controls metabolic homeostasis of carbohydrates and lipids.[37–40] Dysregulation of the IIS pathway can lead to insulin resistance, diabetes, and other metabolic disorders.[41,42] Reducing IIS activity was reported to mediate DR-regulated lifespan extension in worms, flies, and mammals.[37,43,44]

To further understand the role of IIS in brain lipid metabolism during aging, we studied *Drosophila* mutants with reduced functional copies of *chico*, a homolog of insulin receptor substrate. The heterozygous adults with a loss of functional allele, genotypically $chico^{1}$/+, were shown to have extended lifespan and improved locomotor function.[36,45–48] We found that the density and size of brain LDs were reduced significantly in both old female (Fig. 5A and Supplementary Fig. S4A, B) and male $chico^{1}$/+ flies (data not shown). This reduction reflects a decrease of lipid storage in the brain, which could be due to the enhanced lipid turnover.

To verify this, we examined lipid turnover dynamics in $chico^{1}$/+ mutant fly brains. DO-SRS imaging and quantification results indicate that, compared with w^{1118} (+/+) female controls, the CD/CH ratio in LDs increased significantly in both 7-day (by 15%; data not shown) and 35-day (by 85%) female $chico^{1}$/+ fly brains (Fig. 5B). But CD/CH ratio in LDs from males only slightly increased in 7 and 35 days (Fig. 5B and data not shown). These results show that LDs in $chico^{1}$/+ female brain maintained high lipid turnover rate during aging, and IIS reduction changed brain lipid metabolism in a sex-dependent manner.

Of note, label-free SRS images at lipid-related peaks of 2850 cm^{-1} can also detect the lipids on cell membranes (Fig. 5C, D). The lipid-related peaks were also confirmed by SRS hyperspectral images (the sharp peak at 2850 cm^{-1} of the yellow spectrum in Supplementary Fig. S4C). Removing lipids by methanol treatment in brain tissue abolished the lipid signal at 2850 cm^{-1}, but the protein signal at 2930 cm^{-1} remained (Supplementary Fig. S4 C, D). In contrast, removing proteins by proteinase K treatment abolished the peak at 2930 cm^{-1}, highlighting the 2850 cm^{-1} lipid peak (Supplementary Fig. S4C).

These results verified that the lipid signals on cell membranes were not due to the bleed through from protein signal at 2930 cm^{-1}. Interestingly, we found that lipid content of brain membrane was significantly reduced during normal aging process in the control flies, but it was preserved in the $chico^{1}$/+ fly brains (Fig. 5C–E). Together with the smaller LD size and larger lipid turnover in $chico^{1}$/+ flies, we hypothesized that IIS downregulation promoted lipid exchanges between LD and membranes (Fig. 5G).

Downregulation of IIS pathway has been shown to alter metabolic profiles in *Drosophila* fat body and muscle, mainly by activating the downstream transcription factor Dfoxo.[37,49–53] We then examined how brain lipid metabolism was modulated by dFOXO by using loss-of-function transheterozygous mutants, $dfoxo^{\Delta 94}$ and $dfoxo^{25}$ *Drosophila* mutants.[54] Contrary to small LDs observed in $chico^{1}$/+ flies, LDs in *dfoxo* mutants were significantly enlarged compared with control, especially at the old stages (35–45 days) (Fig. 5A and Supplementary S4A, B), which might be due to the increased lipid synthesis or reduced lipolysis. We first checked D_2O labeled lipid turnover in mutants. Interestingly, we found no significant changes of lipid turnover in *dfoxo* females, but it was significantly reduced in males (Fig. 5B).

The enlarged LD size in *dfoxo* mutants reminded us of the inert LDs with reduction of lipolysis in the normal aging brains. We thus examined the lipolytic rate in these *dfoxo* mutants

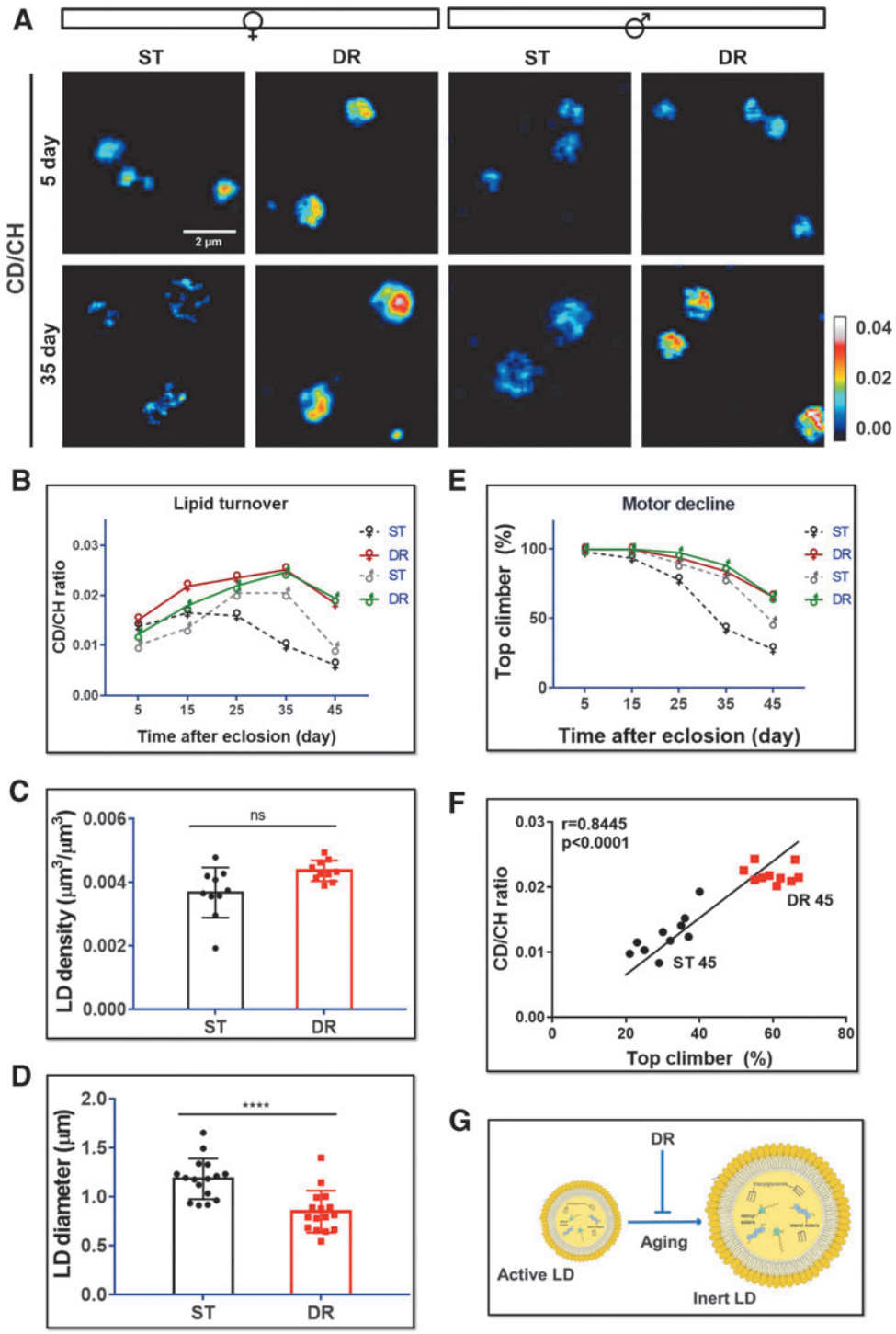

FIG. 4. DO-SRS imaging detected the metabolic changes of brain LDs under DR.

(A) Representative ratiometric images for diet regulated lipid turnover in brain LDs 5- and 35-day female and male flies on standard diet (ST) and DR. Scale bar: 2 μm.

(B) The brain LDs from 5-, 15-, 25-, 35-, and 45-day-old females pretreated with 20% D_2O labeled standard diet (ST) and DR for 5 days were imaged from the CD lipids (2143 cm^{-1}), CH lipids (2850 cm^{-1}), and the ratio of newly synthesized lipids to total lipids (CD/CH) during 5-day D_2O-labeling were quantified and plotted as mean ± SD. $n = 15$ ROIs from 5 to 8 brains.

(C, D) Brain LD density (**C**) and LD size (**D**) in flies fed on ST and DR. Data presented are mean ± SD ($n = 5$–8 brains).

(E) The motor activities of 5-, 15-, 25-, 35-, and 45-day-old flies fed with ST and DR were evaluated and plotted as mean ± SD. $n = 40$ flies for each age group.

(F) A linear positive correlation between brain lipid synthesis and locomotor function of 45-day-old female flies under different diet treatments. $n = 8$ brains for CD/CH quantification, 40 flies for locomotor analysis in each group. Pearson analysis, $r = 0.849$, $p < 0.0001$.

(G) A schematic model showing DR delays the aging process of brain LDs. Statistical significance was determined by using Student's *t*-test. ****$p < 0.0001$; ns, nonsignificant difference; DR, dietary restriction.

using the starvation assay. The lipid mobilization in *dfoxo* mutants was remarkably reduced during 72 h starvation in *dfoxo* mutant flies (Fig. 5F and Supplementary Table S5). We also compared the LD size and lipogenic activities in 0-day (the day flies eclosed from pupae) $dfoxo^{\Delta 94}/dfoxo^{25}$ mutant with control and found no significant differences, suggesting that the change of lipid metabolism was not from development but adult-onset (Supplementary Fig. S4E, F). The data together suggest that enlarged LDs in *dfoxo* mutants were due to the reduced lipid mobilization during aging process.

We further examined brain lipid metabolism in the combined $chico^{1}/+$; $dfoxo^{\Delta 94}/dfoxo^{25}$ mutant flies. The LD size in these flies was enlarged and the LDs had same trend of lipid metabolic activity as $dfoxo^{\Delta 94}/dfoxo^{25}$ mutants (Fig. 5A, B, and F; Supplementary Fig. S4A, B and Supplementary Table S5), suggesting the beneficial effects of downregulated IIS ($chico^{1}/+$) functions

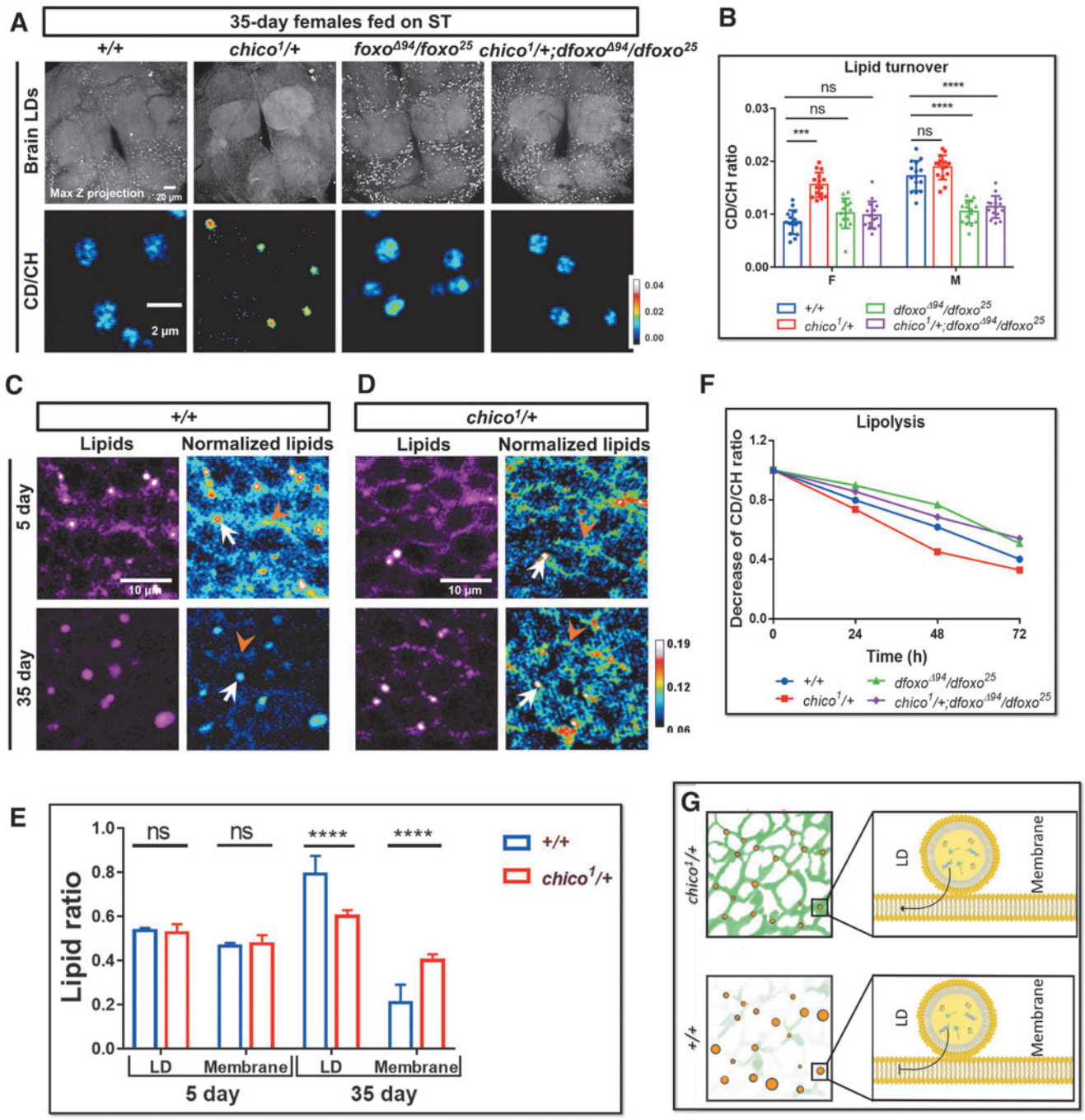

FIG. 5. Brain lipid metabolic changes in IIS mutant flies.

(A) Max Z projected images of the whole-mount brains (upper) and DO-SRS images of brain lipid turnover (lower) from IIS mutants (*chico*^{1}/+, *dfoxo*$^{\Delta 94}$/*dfoxo*^{25} and *chico*^{1}/+; *dfoxo*$^{\Delta 94}$/*dfoxo*^{25}) and control (*w*^{1118}).

(B) Quantification of lipid turnover rates in brain LDs from 7- (young) and 35-day (old) mutants. $n = 15$ ROIs from 3 to 5 brains.

(C, D) The SRS images of 2850 cm^{-1} (magenta; left panels) demonstrate the subcellular distribution of lipids in cell body regions from 5- and 35-day-old control flies (+/+) **(C)** and IIS mutants (*chico*^{1}/+) **(D)**. The ratiometric images of 2850 cm^{-1}/2930 cm^{-1} (royal; right panels) quantitatively map lipid levels in the membranes. White arrows, LDs; orange arrowheads, cell membranes. Scale bar: 10 μm.

(E) The quantification LD lipid ratio (LD lipids/(LD lipids + membrane lipids)) and membrane lipid ratio (membrane lipids/(LD lipids + membrane lipids)) from **(C)** and **(D)**. Data are presented as mean ± SD.

(F) The time-course quantification of CD-lipid mobilization (CD/CH ratio decline) from brain LDs in 10-day IIS mutant flies after 0-, 24-, 48-, and 72-h starvation. Data are presented as mean ± SD. $n = 15$ ROIs from 3 to 5 brains at each group.

(G) A model describing that the reduction in membrane lipids could be reversed by IIS downregulation. The membrane lipids were reduced during normal aging process but were preserved by *chico*^{1} mutant. Statistical significance was determined by using one-way ANOVA in **(B)**, the statistic analysis in **(E)** was determined by using Student's *t*-test. ***$p < 0.001$; ****$p < 0.0001$; ns, nonsignificant difference.

through dFOXO on regulation of brain lipid turnover. The brain turnover gets increased in *chico*^{1} females to a larger extent than males, but it is reduced more in *dfoxo* males than females, suggesting IIS pathway may be involved in regulating the sex differences of brain lipid metabolism.

Bioorthogonal SRS imaging resolved brain metabolic shifts upon DR and IIS manipulations

Glia-specific IIS inhibition was shown to extend lifespan in *Drosophila*.[55] To investigate how lipid metabolic activity was regulated by the glial IIS in adult brain (rather than during development), we applied mifepristone (RU486)-inducible glia-specific Gal4 driver *GSG907* to modulate IIS activity in adult brain by overexpressing Pten (a lipid phosphatase counteracting PI3K enzymatic activity, *GliaGS>UAS-Pten*), and expressing mutant InR including *GliaGS>UAS-InRDN* (the dominant negative form of InR), with *GliaGS>UAS-lacZ* as the control. Both *GliaGS>UAS-Pten* and *GliaGS>UAS-InRDN* flies showed reduced LD density phenotype in the brains (Fig. 6A, B), similar to the *chico*^{1}/+ flies, although to a lesser extent.

We next examined brain lipid metabolic activities in 35-day IIS transgenic flies. DO-SRS ratiometric images and quantification results showed significantly increased lipid turnover rate upon downregulation of IIS activity in both *GliaGS>UAS-Pten* and *GliaGS>UAS-InRDN* females, compared with age- and sex-matched control (*GliaGS>UAS-lacZ*) (Fig. 6A, C). However, there was no significant change of lipid turnover rate in the transgenic males (Fig. 6C), consistent with the aforementioned results that females are more sensitive to systemic IIS downregulation.

Similar with the phenotype of *dfoxo* mutants, we found significantly enlarged LD size and increased LD density in both *GliaGS>UAS-dfoxoRNAi* and *GliaGS>UAS-InRDN,UAS-dfoxoRNAi* flies (Supplementary Fig. S5A). The brain lipid mobilization was reduced in *GliaGS>UAS-dfoxoRNAi* and *GliaGS>UAS-InRDN,UAS-dfoxoRNAi* flies, suggesting that dFOXO knockdown was epistatic to InRDN overexpression (Supplementary Fig. S5B). These results again confirmed dFOXO plays an important role in IIS signaling-mediated regulation of brain lipid metabolism.

Using a neuron-specific *elavGS* driver to downregulate IIS in *elavGS>UAS-InRDN* and *elavGS>UAS-dfoxoRNAi* flies, we found no significant changes in LD density and lipid turnover compared with the *elavGS>UAS-lacZ* control (Supplementary Fig. S5C–E), suggesting neuronal IIS may not play a dominant role in brain lipid turnover. Taken together, our data demonstrate that glia-specific IIS regulates lipid metabolic turnover in *Drosophila* aging brain.

Aforementioned data obtained by DO-SRS imaging have shown that the general lipid metabolic activity was increased by downregulating IIS. Under prolonged DR or reduced IIS activity, it remains unclear how the reprogramming of lipid metabolism sustains neuronal survival and to what extent other metabolites, such as acetate and glutamine, contribute to support neurons. We next determined the metabolic origin of glial LDs by using SRS imaging combined with another two bioorthogonal probes, deuterated (D)-glucose and D-acetate, respectively.

Flies were cultured on diets containing D-glucose or D-acetate, major carbon sources for lipogenesis. The lipogenesis in glial LDs was then examined. SRS imaging revealed strong deuterium incorporation from dietary D-glucose or D-acetate into the core of LDs (Fig. 6D). CD/CH ratios in brain cross sections were quantified. The D-acetate-derived lipids were increased in the flies manipulated by DR and IIS downregulation. Meanwhile, D-glucose-derived lipids were significantly reduced upon IIS downregulation, even though no obvious changes were found in DR flies (Fig. 6D, E).

These results suggested that brain metabolism shifted toward using acetate as a major source for lipogenesis under DR or glia-specific IIS downregulation (Fig. 6F). In this study, we hypothesized that when IIS activity was downregulated, the precursor for lipid synthesis, acetyl-CoA, was mainly generated from acetyl-CoA synthetase (ACSS)-mediated pathway, rather than glycolysis-ATP citrate lyase (ACLY)-dependent pathway.[56]

Discussion

For the first time we employed DO-SRS imaging to directly visualize and quantify spatiotemporal changes of lipid metabolic activity at organelle level (1–2 μm LD) in aging *Drosophila* brain. We examined interconnections between brain lipid metabolism, sex differences, dietary regulation, IIS pathway, and locomotor activity.

We observed abundant metabolically active small LDs and lipid rich membranes in young *Drosophila* brains. However, the LDs became enlarged and metabolically inert, whereas membrane lipids were reduced in the aged brains. Previous studies showed fatty acids from membrane phospholipids could redistribute to LDs during oxidative stress,[14,57] suggesting active interaction between LDs and membranes. Our study suggested that lipid exchanges between LD storage and membranes were likely impaired in the aged brain, leading to lipid misallocation from membranes to LDs,[58,59] which could be reversed by IIS downregulation.

Our results also demonstrated that regulation of lipid storage in the brain is a highly dynamic process, similar to that in the adipose tissue,[20] which is balanced between lipid synthesis and mobilization in LDs. Aging affected more than the process of lipogenesis, lipolysis, and translocation, but lipid shuttling between glia and neurons is also important to maintain brain energy homeostasis and function.[11,60–66] Brain lipid homeostasis was intimately bound up with oxidative stress, injury, and immune challenges during aging process.[10,12–14] Dysregulation of brain lipid metabolism can cause or accelerate brain aging and neurodegenerative diseases. Our *in vivo* SRS imaging of lipid metabolic dynamics at subcellular level could provide insights into the underlying mechanisms of aging-dependent neurodegenerative diseases.

We found remarkably improved lipid turnover under DR and IIS manipulations, as well as positive correlation between brain lipid turnover and locomotor activity. DR and the IIS pathway have been shown to regulate lipid metabolism and reduce the accumulation of harmful lipids, such as lipid peroxide.[67] Our study indicates that the improvement on brain lipid turnover or lipid translocation from LD to membrane could contribute to lifespan extension, as observed under DR and reduced IIS

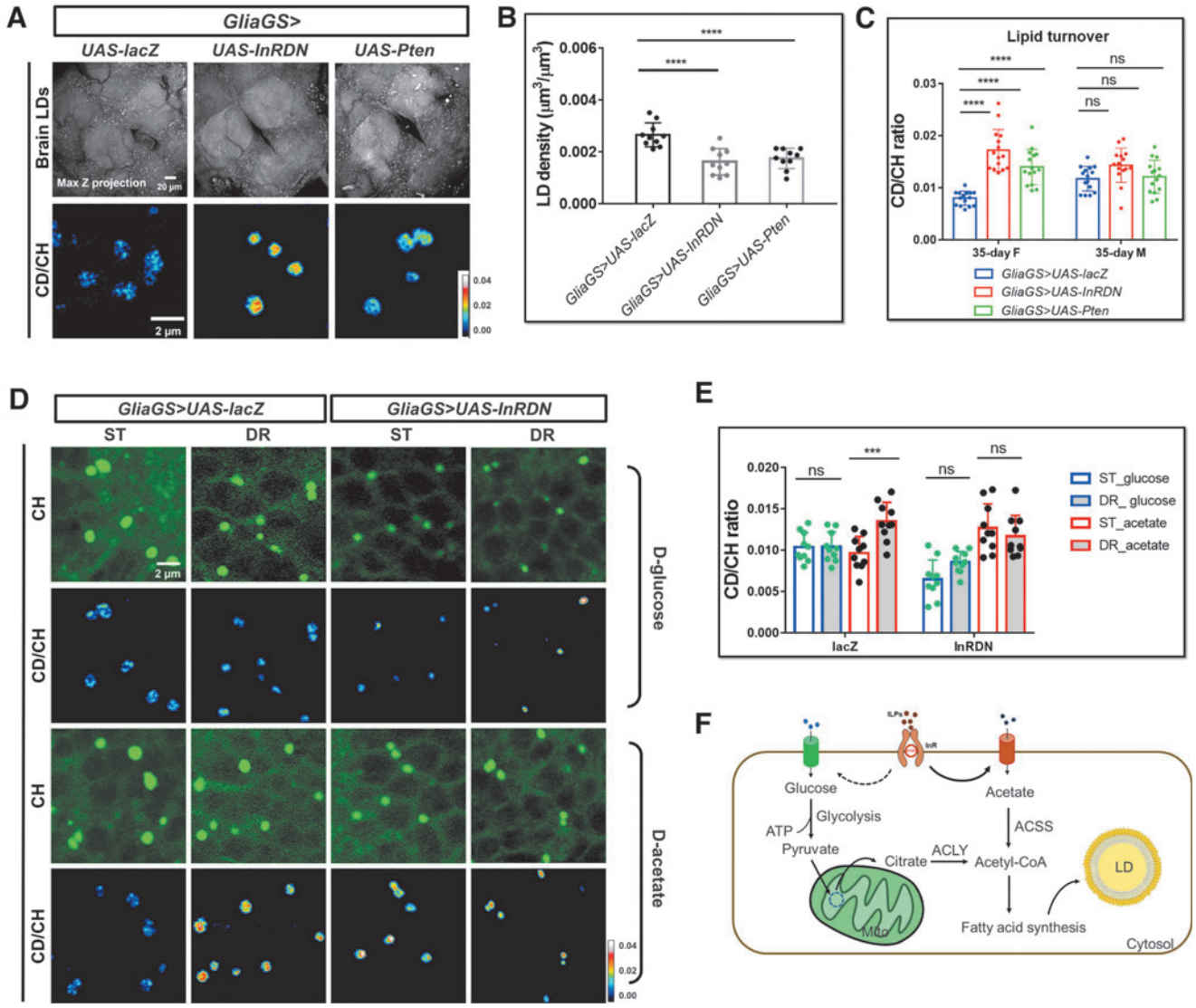

FIG. 6. Bioorthogonal SRS imaging revealed the brain metabolic shifts upon DR and IIS manipulations.

(A) Max Z projected images of whole-mount brain and DO-SRS images of brain lipid turnover (lower) from glia-specific gene manipulated (*GliaGS*>) adult flies (*UAS-InRDN* and *UAS-Pten*) are compared with that of *GliaGS*>*UAS-lacZ*.

(B) LD density (total LD volume to brain cortex volume) in (**A**, upper) was quantified and presented as mean ± SD. $n = 5$ brains in each group. **(C)** The lipid turnover rates (CD/CH) in (**A**, lower) were quantified and plotted as mean ± SD. $n = 15$ ROIs from 3 to 5 brains in each group.

(D) DO-SRS images of brain lipid turnover labeled by D-glucose and D-acetate were taken from glia-specific gene-manipulated (*GliaGS*>) adult flies (*UAS-lacZ*, *UAS-InRDN*, and *UAS-Pten*). These flies were fed with standard diet or under DR.

(E) Quantification of D-glucose and D-acetate probed lipid turnover rates (CD/CH) of brain LDs from **(D)**. Data are presented as mean ± SD. $n = 15$ ROIs from 3 to 5 brains.

(F) A working model describing IIS pathway-mediated metabolic shift. Acetyl-CoA is the precursor for lipid synthesis. When IIS activity was downregulated, acetyl-CoA generated through glycolysis and ACLY was reduced, whereas the metabolic pathway leaning toward ACSS mediated acetyl-CoA generation. Statistical significance in **(B)**, **(C)**, and **(E)** was determined by using one-way ANOVA. ***$p < 0.001$; ****$p < 0.0001$; ns, nonsignificant difference. ACLY, ATP citrate lyase; ACSS, acetyl-CoA synthetase.

activity. However, more research is needed to fully understand the complex interactions between lipid metabolism and these pathways as well as their effects on aging and health span.

Previous studies showed that insulin receptor expression in glia is critical for brain function.[39,68] Inhibition or downregulation of IIS specifically in glia extended the lifespan.[55,69] It underscored the crucial role of brain lipid metabolism in maintaining not only nervous system function but also organism-wide health. dFOXO was supposed to mediate the health span extension from IIS downregulation.[49,50,52,70] CNS-specific deletion of

FoxO3 in 5xFAD mice led to altered brain lipid levels and exacerbation of synaptic loss and Abeta pathology, whereas astrocyte-specific overexpression of FoxO3 reversed these neurodegenerative phenotypes, suggesting a neuroprotective role of FoxO3.[71]

The single-cell RNA-sequencing profiling of the adult *Drosophila* brain also showed that FOXO is endogenously expressed in glia but not neurons.[72,73] Our study showed that glial downregulation of IIS activity enhanced lipid turnover and rejuvenated the enlarged inert LDs to small active ones in old animals. However, glia-specific knockdown of *dfoxo* is sufficient to deactivate the lipid turnover, resulting in larger LD size and number. These findings engender us to understand the underlying mechanism of glia IIS-regulated brain lipid metabolism. Whether inert LD-loaded glia have the same identity as the pathological microglia,[12] and are involved in age-related and genetic forms of neurodegeneration remains to be investigated.

It has been shown that IIS is low when nutrients are sparse and dFOXO translocate nuclear to active the downstream genes' expression.[74] Our results show sexual dimorphism in brain lipid metabolism during normal aging, diets, and IIS manipulations, consistent with those observed in peripheral tissues.[35,75,76] It suggests the IIS sensitivity in brain is different between females and males. It has been reported that DR treatment exerted significant effects on extending lifespan in female flies more than male flies. And IIS plays a sex-dependent role in the body size and locomotor activity.[47,77–81] How the lipid metabolism in local glia IIS is determined, and the correlation between IIS sensitivity, lipid turnover, and health span await more future studies.

In this study with bioorthogonal SRS imaging, we found acetate, instead of glucose, -derived lipids were largely increased under DR or reduced IIS activity. This acetate-mediated lipogenesis has been reported to promote cancer cell survival under stresses.[82–85] However, the mechanism behind this metabolic shift and its role in DR/IIS-mediated lifespan extension needs further study.

Our study indicates that lipid turnover plays a crucial role in brain metabolic homeostasis and animal aging; however, the functions of different subtypes of glia and neurons in regulating brain lipid metabolism and healthy lifespan remain to be further determined. In addition to IIS-dFOXO axis, other signal pathways or factors may also participate in brain metabolic regulations.[66,86,87] Our *in situ* metabolic imaging method will be highly useful to directly visualize and quantify the spatiotemporal alterations of metabolic profiles and to cast light on understanding the mechanisms underlying brain aging and diseases.

The Bigger Picture

Lipid metabolism plays an important role in brain aging and is associated with aging-related neurodegenerative diseases such as Alzheimer's disease (AD), dementia, Parkinson's disease (PD). Dietary, pharmacological, and genetic interventions of different lipid subtypes have been shown to extend the lifespan of a variety of animals. Disturbances of lipids composition or dysregulation of lipids metabolism may contribute to a series of abnormalities in brain functions such as rupture of the blood-brain barrier, disturbed myelination, and abnormal amyloid precursor protein processing, which are hallmarks of AD. Understand how lipid metabolism plays in aging and neurodegenerative diseases could pave the way for early diagnosis, prevention, and effective treatments of these diseases. However, many underlying molecular mechanisms are still to be revealed.

High resolution spatiotemporal mapping of lipids dynamics regulated by dietary composition, insulin/IGF-1 signaling (IIS) pathway, and aging offers a novel approach for unraveling the mechanisms. Our DO-SRS imaging approach provides a novel and powerful tool to directly visualize new lipid synthesis in the brain. With high subcellular resolution and fast imaging speed, it is able to track and map spatiotemporal distribution of lipids metabolic dynamics in cells in brain and many other tissues in situ, for unraveling the interconnections between lipids metabolism, activity of insulin signaling (IIS) pathway, and dietary compositions on brain aging and age-related diseases such as dementia, AD, PD. Further combined with other deuterium labeled metabolites such as deuterated amino acids and glucose,[88,89] and imaging processing techniques such as the adaptive moment estimation (Adam) optimization-based pointillism deconvolution (A-PoD) and penalized reference matching (PRM) algorithms,[26,90] SRS imaging can measure and identify a variety of nanoscopic colocalized lipids subtypes, as well as other biomolecules such as proteins and DNAs, in organelles, which manifests broad application of DO-SRS-based technique in multiplex cell and tissue imaging in life science.

Materials and Methods

Drosophila genetics

Fly lines used in this study were originally obtained from the Bloomington *Drosophila* Stock Center (BDSC) unless otherwise stated. They have been maintained on standard diet (Nutri-Fly, Cat. No. 66-113; Genesee Scientific Corporation) in the laboratory for several generations. The wild type used for normal aging and diet treatment was w^{1118} (stock #5905).

Genetic elements used were *repo-Gal4* (stock #7415), *GliaGS-Gal4* (*GSG550*, stock #62085 or *GSG907*, stock #40310), *elavGS- Gal4* (kindly provided by Dr. Xu Chen), *UAS-lacZ* (stock #8530), *UAS-InRCA* (also known as *InRdel*, stock #8248), *UAS-InR.DN* (stock #8253), *UAS-Pten* (stock #82170), *UAS-ACC RNAi* (stock #34885), *UAS-white RNAi* (was crossed out from stock #65409), *UAS-LpR1 RNAi* (stock #50737), *UAS-LpR2 RNAi* (stock #54461), *UAS-Lipin* RNAi (stock #63614), *UAS-DGAT1RNAi* (stock #65963), *UAS-Bmm* (stock #76600), and *UAS-dfoxo RNAi* (stock #32427). IIS pathway mutant alleles and reporter used were $chico^{1}$ (stock #10738), $dfoxo^{25}$ (stock #80944), $dfoxo^{\Delta 94}$ (stock #42220), and dFOXO-GFP (stock #38644).

SRS microscopy and hyperspectral imaging

The SRS and SRS-HSI images were collected from an upright laser-scanning microscope (DIY multiphoton; Olympus). It was equipped with a 25× water objective (XLPLN, WMP2, 1.05 NA; Olympus), which was applied for near-IR throughput. The synchronized pulsed pump beam (tunable 720–990 nm wavelength, 5–6 ps pulse width, and 80 MHz repetition rate) and stokes beam (wavelength at 1032 nm, 6

ps pulse width, and 80 MHz repetition rate) were supplied by a picoEmerald system (Applied Physics & Electronics) and coupled into the microscope. After interacting with the samples, the pump and Stokes beams were collected in transmission by a high NA oil condenser (1.4 NA).

A high O.D. shortpass filter (950 nm; Thorlabs) was used to completely block the Stokes beam and transmit the pump beam only onto a Si photodiode for detecting the stimulated Raman loss signal. The output current from the photodiode was terminated, filtered, and demodulated by a lock-in amplifier at 20 MHz. The demodulated signal was fed into the FV3000 software module FV-OSR (Olympus) to form image using laser scanning. All images obtained were 512×512 pixels, with a dwell time 80 μs and imaging speed of $\sim$23 s per image. A background image was acquired at 2190 cm^{-1} and subtracted from all SRS images using ImageJ. The hyperspectral imaging stack of brain was taken at 75 spectral points covering 2800–3150 cm^{-1} at 40 μs pixel dwell time, then intensity profiles of interested regions were plotted in ImageJ.

LD analysis

3D *Drosophila* brain images were taken by SRS imaging system at 2850 cm^{-1}. To enhance the detection precision, the pixel numbers were increased by two times along the lateral direction and four times along the axial direction and then A-PoD[26] was used to convert the preprocessed 3D images to the super-resolved images. From the super-resolved image, the numbers and sizes of LDs were measured with the 3D objects counter plugin[91] of ImageJ.

The information about volume and location of each LD were exported and delivered to a home-built Matlab code to visualize the data as color-coded 3D images. To reduce the background noise, band pass filter (threshold: 50 px) was applied to filtering high-frequency signal. The profile of the CBs including neuropiles was delineated by FeatureJ structure plugin.[92] The color-coded LD images and CB areas are combined into a single image stack to present the 3D distribution of each LD in the *Drosophila* brain.

Diet manipulation and locomotor function assay

The w^{1118} parents were raised in vials containing standard diet. To standardize the effects of parental age on offspring fitness, parents of experimental flies were of the same age (4–5 days and reared at a constant density for at least two generations). To synchronize larval development, we allowed flies to lay eggs on yeast apple juice plates for 1 h, discarded the first batch of embryos, and then collected for another 4 h. Groups of 20–25 embryos were put into vials containing standard diet and allowed to develop until pupae eclosion.

Newly eclosed flies were allowed to mature and mate for 48 h before the flies were briefly anesthetized with CO_2 so that females and males could be separated for aging experiments. One hundred adult flies were randomly allocated at a density of 20 flies per vial using four cohorts for each diet: standard diet (ST), DR. For the detailed information of the food recipe (Supplementary Table S1). All eclosures were maintained at 25°C in a controlled light (12/12-h light/dark cycle) and humidity (>70%) environment. Flies were scored for survival daily and provided with fresh medium every 2 days. To minimize any density effects on mortality, two vials with cohorts were merged when the density of flies reached five or fewer individuals.

Eclosures were placed randomly in the incubator, and positions were rotated after each transfer to minimize the effects of microclimate. This process was followed until the end of experiments. The locomotor functions of flies were determined as reported.[93] Parental flies (w^{1118}) were kept for 15 females and 10 males per vial and flipped every 2 days to prevent overcrowding. Progeny flies were collected within 24 h of eclosion and aged without further CO_2 exposure. After 2 days' maturation, females and males were separated to different groups. For each diet condition, six vials of each sex with 20 flies per vial (totally 120 females, 120 males) were set up for examining the changes of motor activities during aging process.

The assay was performed approximately at the same time during the daytime to minimize circadian differences. Flies were transferred to the glass cylindrical vials with a line at the 5 cm mark and allowed to acclimate the circumstance for 10–15 min before testing. Flies were gently tapped down to the bottom of the vial, and the percentage of flies that crossed the 5 cm mark in 30 s was determined. Vials were placed horizontally and flies were retested 10–15 min later. The average of the two technical replicates for each vial was recorded and was plotted as a single point. The locomotor function was at 5, 15, 25, 35, and 45 days after eclosion.

D_2O-labeling experiments

The changes of lipid turnover rated in wild-type flies at different ages were labeled by transferring the 0-, 10-, 20-, 30-, and 35-day adult flies to the 20% D2O labeled corresponding food conditions for 5 days, then the 5-, 15-, 25-, 35-, and 45-day aged flies were sacrificed, and their brains were dissected and subjected to Raman measurements and SRS imaging.

For investigating the metabolic activity of the IIS-related gene mutants, $chico^{1}$/+ and $dfoxo^{\Delta 94}/dfoxo^{25}$ flies aged at 2 days (young) and 30 days (old) were labeled by 20% D_2O labeled for 5 days, then the 7- and 35-day aged flies were sacrificed, and their brains were dissected and subjected to Raman measurements and SRS imaging, respectively. The age paired w^{1118}(+/+) flies treated in the same way were used as control.

For determining the metabolic activity of glia-specific IIS manipulated transgenic flies. Groups of 15 *GliaGS* virgin females were collected to cross with 15 *UAS-InRDN, UAS-Pten of UAS-dfoxo RNAi* males, respectively. All the crosses were maintained at 21°C on the standard diet to allow the normal embryo and larvae development. Eighty newly eclosed progenies (40 females and 40 males) with correct genotype were collected.

They were allocated to four cohorts (20 flies of each) and transferred to fresh food with RU-486 (Cat. No. 84371-65-3; Sigma) added at a final concentration of 200 μM and raised in 25°C. After 2 days maturation and mating, the 15 females and 15 males were separated and subjected to 5 day 20% D_2O labeling experiments, then the brains from 7-day aged flies were dissected and measured by Raman or SRS imaging system. The rest of the flies (25 females and 25 males) were allowed to grow old to 30 days for D_2O treatment and following experiments.

For the starvation assay, four groups of 2-/20-day old adult flies (15 flies per group) were transferred to fresh vials with 20% D_2O labeled diets for 10 days labeling. Then the labeled (12- and 30-day) flies were starved on 1% agar. At each time point (24, 48, and 72 h after starvation), five flies randomly selected from the four vials were sacrificed, and brains were dissected and subjected to SRS imaging for the C–D signal quantification. The CD/CH ratios of LDs from three regions of interest in each brain were measured by ImageJ software and then the quantifications from 5 to 10 brains at each group were used to do statistical analysis.

D-glucose and D-acetate labeling experiments

Flies were fed isocaloric diets containing D-glucose (2 mM) and D-acetate (1 mM) (Cambridge Isotope Laboratories) for 5 days and the brains were dissected and subjected to SRS imaging.

Brain LD staining

Brains were fixed overnight in 4% paraformaldehyde in phosphate-buffered saline (PBS) in 4°C, then washed three times with PBS. One

microgram per milliliter BODIPY 493/503 (Cat. No. D3922; Invitrogen™) was used as final concentration to stain overnight in 4°C. After one rinse in PBS, tissues were rinsed and mounted in PBS for two photon fluorescent imaging at 800 nm wavelength.

Statistical analysis

Statistical significance was tested by using Student's *t*-test, one-way or two-way analysis of variance (ANOVA) with Tukey's multiple comparison or Dunnett's comparison using GraphPad Prism software. Kaplan–Meier log-rank test was performed for survival assays. *$p < 0.05$; **$p < 0.01$; ***$p < 0.001$; ****$p < 0.0001$; ns, nonsignificant difference.

Acknowledgments

We are grateful to Bloomington Drosophila Stock Center (BDSC) for fly stocks. We thank Drs. K. Zhang, C. Metallo, G. Haddad, D. Zhou, and Shi Lab group members for helpful discussions.

Authors' Contributions

L.S. and Y.L. conceived the idea, designed the study, interpreted data, and wrote the article. Y.L. conducted the experiments, analyzed the data, and performed statistical analyses with the help from P.C., S.S., H.J., Y.N., A.Z., S.H., J.Y.W., X.C., and L.S. Y.L., J.Y.W., and L.S. wrote and revised the article.

Author Disclosure Statement

No competing financial interests exist.

Funding Information

We acknowledge support from UCSD Startup funds, NIH U54 2U54CA132378, NIH 5R01NS111039, NIH R21NS125395, Sloan Research Fellow, and Hellman Fellow Award.

Supplementary Material

Supplementary Figure S1
Supplementary Figure S2
Supplementary Figure S3
Supplementary Figure S4
Supplementary Figure S5
Supplementary Table S1
Supplementary Table S2
Supplementary Table S3
Supplementary Table S4
Supplementary Table S5

References

1. Kirkwood TB, Austad SN. Why do we age? Nature 2000;408(6809):233–238; doi: 10.1038/35041682
2. Chung KW. Advances in understanding of the role of lipid metabolism in aging. Cells 2021;10(4):880; doi: 10.3390/cells10040880
3. Bruce KD, Zsombok A, Eckel RH. Lipid processing in the brain: A key regulator of systemic metabolism. Front Endocrinol (Lausanne) 2017;8:60; doi: 10.3389/fendo.2017.00060
4. Denis I, Potier B, Heberden C, et al. Omega-3 polyunsaturated fatty acids and brain aging. Curr Opin Clin Nutr Metab Care 2015;18(2):139–146; doi: 10.1097/MCO.0000000000000141.
5. Cutuli D. Functional and structural benefits induced by omega-3 polyunsaturated fatty acids during aging. Curr Neuropharmacol 2017;15(4):534–542; doi: 10.2174/1570159X14666160614091311
6. Chiu CC, Su KP, Cheng TC, et al. The effects of omega-3 fatty acids monotherapy in Alzheimer's disease and mild cognitive impairment: A preliminary randomized double-blind placebo-controlled study. Prog Neuropsychopharmacol Biol Psychiatry 2008;32(6):1538–1544; doi: 10.1016/j.pnpbp.2008.05.015
7. Janssen CI, Kiliaan AJ. Long-chain polyunsaturated fatty acids (LCPUFA) from genesis to senescence: The influence of LCPUFA on neural development, aging, and neurodegeneration. Prog Lipid Res 2014;53:1–17; doi: 10.1016/j.plipres.2013.10.002
8. Tindale LC LS, Spinelli JJ, Brooks-Wilson AR. Lipid and Alzheimer's disease genes associated with healthy aging and longevity in healthy oldest-old. Oncotarget 2017;8(13):20612–20621; doi: 10.18632/oncotarget.15296
9. Hussain G, Wang J, Rasul A, et al. Role of cholesterol and sphingolipids in brain development and neurological diseases. Lipids Health Dis 2019;18(1):26; doi: 10.1186/s12944-019-0965-z
10. Kis V, Barti B, Lippai M, et al. Specialized cortex glial cells accumulate lipid droplets in Drosophila melanogaster. PLoS One 2015;10(7):e0131250; doi: 10.1371/journal.pone.0131250
11. Ioannou MS, Jackson J, Sheu SH, et al. Neuron-astrocyte metabolic coupling protects against activity-induced fatty acid toxicity. Cell 2019;177(6):1522–1535 e14; doi: 10.1016/j.cell.2019.04.001
12. Marschallinger J, Iram T, Zardeneta M, et al. Lipid-droplet-accumulating microglia represent a dysfunctional and proinflammatory state in the aging brain. Nat Neurosci 2020;23(2):194–208; doi: 10.1038/s41593-019-0566-1
13. Liu L, Zhang K, Sandoval H, et al. Glial lipid droplets and ROS induced by mitochondrial defects promote neurodegeneration. Cell 2015;160(1–2):177–190; doi: 10.1016/j.cell.2014.12.019
14. Bailey AP, Koster G, Guillermier C, et al. Antioxidant role for lipid droplets in a stem cell niche of drosophila. Cell 2015;163(2):340–353; doi: 10.1016/j.cell.2015.09.020
15. Liu L, MacKenzie KR, Putluri N, et al. The glia-neuron lactate shuttle and elevated ROS promote lipid synthesis in neurons and lipid droplet accumulation in glia via APOE/D. Cell Metab 2017;26(5):719–737 e6; doi: 10.1016/j.cmet.2017.08.024
16. Piper MD, Partridge L, Raubenheimer D, et al. Dietary restriction and aging: A unifying perspective. Cell Metab 2011;14(2):154–160; doi: 10.1016/j.cmet.2011.06.013
17. Raubenheimer D, Simpson SJ, Le Couteur DG, et al. Nutritional ecology and the evolution of aging. Exp Gerontol 2016;86:50–61; doi: 10.1016/j.exger.2016.04.007
18. Senior AM, Legault V, Lavoie FB, et al. Multidimensional associations between nutrient intake and healthy ageing in humans. BMC Biol 2022;20(1):196; doi: 10.1186/s12915-022-01395-z
19. Shi L, Zheng C, Shen Y, et al. Optical imaging of metabolic dynamics in animals. Nat Commun 2018;9(1):2995; doi: 10.1038/s41467-018-05401-3
20. Li Y, Zhang W, Fung AA, et al. DO-SRS imaging of diet regulated metabolic activities in Drosophila during aging processes. Aging Cell 2022;21(4):e13586; doi: 10.1111/acel.13586
21. Ugur B, Chen K, Bellen HJ. Drosophila tools and assays for the study of human diseases. Dis Model Mech 2016;9(3):235–244; doi: 10.1242/dmm.023762
22. De Gelder J, De Gussem K, Vandenabeele P, et al. Reference database of Raman spectra of biological molecules. J Raman Spectrosc 2007;38(9):1133–1147; doi: 10.1002/jrs.1734
23. Svennerholm L, Boström K, Helander CG, et al. Membrane lipids in the aging human brain. J Neurochem 1991;56(6):2051–2059; doi: 10.1111/j.1471-4159.1991.tb03466.x
24. Svennerholm L, Boström K, Jungbjer B, et al. Membrane lipids of adult human brain: Lipid composition of frontal and temporal lobe in subjects of age 20 to 100 years. J Neurochem 1994;63(5):1802–1811; doi: 10.1046/j.1471-4159.1994.63051802.x
25. Orringer DA, Pandian B, Niknafs YS, et al. Rapid intraoperative histology of unprocessed surgical specimens via fibre-laser-based stimulated Raman scattering microscopy. Nat Biomed Eng 2017;1:0027; doi: 10.1038/s41551-016-0027
26. Jang H, Li Y, Fung AA, Bagheri P, et al. Super-resolution SRS microscopy with A-PoD. Nat Methods 2023;20(3):448–458; doi: 10.1038/s41592-023-01779-1
27. Olzmann JA, Carvalho P. Dynamics and functions of lipid droplets. Nat Rev Mol Cell Biol 2019;20(3):137–155; doi: 10.1038/s41580-018-0085-z
28. Samuel AZ, Miyaoka R, Ando M, et al. Molecular profiling of lipid droplets inside HuH7 cells with Raman micro-spectroscopy. Commun Biol 2020;3(1):372; doi: 10.1038/s42003-020-1100-4
29. Walther TC, Farese RV, Jr. Lipid droplets and cellular lipid metabolism. Annu Rev Biochem 2012;81:687–714; doi: 10.1146/annurev-biochem-061009-102430

30. Musselman LP, Kuhnlein RP. Drosophila as a model to study obesity and metabolic disease. J Exp Biol 2018;221(Pt Suppl 1):jeb163881; doi: 10.1242/jeb.163881
31. van Dam E, van Leeuwen LAG, Dos Santos E, et al. Sugar-induced obesity and insulin resistance are uncoupled from shortened survival in Drosophila. Cell Metab 2020;31(4):710–725 e7; doi: 10.1016/j.cmet.2020.02.016
32. Galenza A, Foley E. A glucose-supplemented diet enhances gut barrier integrity in Drosophila. Biol Open 2021;10(3):bio056515; doi: 10.1242/bio.056515
33. Oka M, Suzuki E, Asada A, et al. Increasing neuronal glucose uptake attenuates brain aging and promotes life span under dietary restriction in Drosophila. iScience 2021;24(1):101979; doi: 10.1016/j.isci.2020.101979
34. Galenza A, Hutchinson J, Campbell SD, et al. Glucose modulates Drosophila longevity and immunity independent of the microbiota. Biol Open 2016;5(2):165–173; doi: 10.1242/bio.015016
35. Wu Q, Yu G, Cheng X, et al. Sexual dimorphism in the nutritional requirement for adult lifespan in Drosophila melanogaster. Aging Cell 2020;19(3):e13120; doi: 10.1111/acel.13120
36. Martin I, Grotewiel MS. Distinct genetic influences on locomotor senescence in Drosophila revealed by a series of metrical analyses. Exp Gerontol 2006;41(9):877–881; doi: 10.1016/j.exger.2006.06.052
37. Partridge L, Alic N, Bjedov I, et al. Ageing in Drosophila: The role of the insulin/Igf and TOR signalling network. Exp Gerontol 2011;46(5):376–381; doi: 10.1016/j.exger.2010.09.003
38. Haselton A, Sharmin E, Schrader J, et al. Partial ablation of adult Drosophila insulin-producing neurons modulates glucose homeostasis and extends life span without insulin resistance. Cell Cycle 2010;9(15):3063–3071; doi: 10.4161/cc.9.15.12458
39. Liu J, Speder P, Brand AH. Control of brain development and homeostasis by local and systemic insulin signalling. Diabetes Obes Metab 2014;16 Suppl 1:16–20; doi: 10.1111/dom.12337
40. Sousa-Nunes R, Yee LL, Gould AP. Fat cells reactivate quiescent neuroblasts via TOR and glial insulin relays in Drosophila. Nature 2011;471(7339):508–512; doi: 10.1038/nature09867
41. Musselman LP, Fink JL, Narzinski K, et al. A high-sugar diet produces obesity and insulin resistance in wild-type Drosophila. Dis Model Mech 2011;4(6):842–849; doi: 10.1242/dmm.007948
42. Pasco MY, Leopold P. High sugar-induced insulin resistance in Drosophila relies on the lipocalin Neural Lazarillo. PLoS One 2012;7(5):e36583; doi: 10.1371/journal.pone.0036583
43. van Heemst D. Insulin, IGF-1 and longevity. Aging Dis 2010;1(2):147–157.
44. Zid BM, Rogers AN, Katewa SD, et al. 4E-BP extends lifespan upon dietary restriction by enhancing mitochondrial activity in Drosophila. Cell 2009;139(1):149–160; doi: 10.1016/j.cell.2009.07.034
45. Clancy DJ, Gems D, Harshman LG, et al. Extension of life-span by loss of CHICO, a Drosophila insulin receptor substrate protein. Science 2001;292:104–106; doi: 10.1126/science.1057991
46. Deng J, Yang M, Chen Y, et al. FUS interacts with HSP60 to promote mitochondrial damage. PLoS Genet 2015;11(9):e1005357; doi: 10.1371/journal.pgen.1005357
47. Belgacem YH, Martin JR. Disruption of insulin pathways alters trehalose level and abolishes sexual dimorphism in locomotor activity in Drosophila. J Neurobiol 2006;66(1):19–32; doi: 10.1002/neu.20193
48. Bai H, Post S, Kang P, et al. Drosophila longevity assurance conferred by reduced insulin receptor substrate chico partially requires d4eBP. PLoS One 2015;10(8):e0134415; doi: 10.1371/journal.pone.0134415
49. Lee S, Dong HH. FoxO integration of insulin signaling with glucose and lipid metabolism. J Endocrinol 2017;233(2):R67–R79; doi: 10.1530/JOE-17-0002
50. Demontis F, Perrimon N. FOXO/4E-BP signaling in Drosophila muscles regulates organism-wide proteostasis during aging. Cell 2010;143(5):813–825; doi: 10.1016/j.cell.2010.10.007
51. Dionne MS, Pham LN, Shirasu-Hiza M, et al. Akt and FOXO dysregulation contribute to infection-induced wasting in Drosophila. Curr Biol 2006;16(20):1977–1985; doi: 10.1016/j.cub.2006.08.052
52. Giannakou ME, Goss M, Junger MA, et al. Long-lived Drosophila with overexpressed dFOXO in adult fat body. Science 2004;305(5682):361; doi: 10.1126/science.1098219
53. Isao Shimokawa TK, Nobutaka Hayashi, Sang-Eun Kim, et al. The life-extending effect of dietary restriction requires Foxo3 in mice. Aging Cell 2015;14(4):707–79; doi: 10.1111/acel.12340
54. Cathy Slack MEG, Andrea Foley, Martin Goss, et al. dFOXO-independent effects of reduced insulin-like signaling in Drosophila. Aging Cell 2011;10(5):735–748; doi: 10.1111/j.1474-9726.2011.00707.x
55. Woodling NS, Rajasingam A, Minkley LJ, et al. Independent glial subtypes delay development and extend healthy lifespan upon reduced insulin-PI3K signalling. BMC Biol 2020;18(1):124; doi: 10.1186/s12915-020-00854-9
56. Zhao S, Torres A, Henry RA, et al. ATP-citrate lyase controls a glucose-to-acetate metabolic switch. Cell Rep 2016;17(4):1037–1052; doi: 10.1016/j.celrep.2016.09.069
57. Welte MA, Gould AP. Lipid droplet functions beyond energy storage. Biochim Biophys Acta Mol Cell Biol Lipids 2017;1862(10 Pt B):1260–1272; doi: 10.1016/j.bbalip.2017.07.006
58. Moghadam NN, Holmstrup M, Pertoldi C, et al. Age-induced perturbation in cell membrane phospholipid fatty acid profile of longevity-selected Drosophila melanogaster and corresponding control lines. Exp Gerontol 2013;48(11):1362–1368; doi: 10.1016/j.exger.2013.08.018
59. van Meer G, Voelker DR, Feigenson GW. Membrane lipids: Where they are and how they behave. Nat Rev Mol Cell Biol 2008;9(2):112–124; doi: 10.1038/nrm2330
60. Van Den Brink DM, Cubizolle A, Chatelain G, et al. Physiological and pathological roles of FATP-mediated lipid droplets in Drosophila and mice retina. PLoS Genet 2018;14(9):e1007627; doi: 10.1371/journal.pgen.1007627
61. Schulz JG, Laranjeira A, Van Huffel L, et al. Glial beta-oxidation regulates Drosophila energy metabolism. Sci Rep 2015;5:7805; doi: 10.1038/srep07805
62. Qi G, Mi Y, Shi X, et al. ApoE4 impairs neuron-astrocyte coupling of fatty acid metabolism. Cell Rep. 2021;34(1):108572; doi: 10.1016/j.celrep.2020.108572
63. Ralhan I, Chang CL, Lippincott-Schwartz J, et al. Lipid droplets in the nervous system. J Cell Biol 2021;220(7):202102136; doi: 10.1083/jcb.202102136
64. Ramosaj M, Madsen S, Maillard V, et al. Lipid droplet availability affects neural stem/progenitor cell metabolism and proliferation. Nat Commun 2021;12(1):7362; doi: 10.1038/s41467-021-27365-7
65. Mou Y, Dong Y, Chen Z, et al. Impaired lipid metabolism in astrocytes underlies degeneration of cortical projection neurons in hereditary spastic paraplegia. Acta Neuropathol Commun 2020;8(1):214; doi: 10.1186/s40478-020-01088-0
66. Yin J, Spillman E, Cheng ES, et al. Brain-specific lipoprotein receptors interact with astrocyte derived apolipoprotein and mediate neuron-glia lipid shuttling. Nat Commun 2021;12(1):2408; doi: 10.1038/s41467-021-22751-7
67. Scherer T, Sakamoto K, Buettner C. Brain insulin signalling in metabolic homeostasis and disease. Nat Rev Endocrinol 2021;17(8):468–483; doi: 10.1038/s41574-021-00498-x
68. Garcia-Caceres C, Quarta C, Varela L, et al. Astrocytic insulin signaling couples brain glucose uptake with nutrient availability. Cell 2016;166(4):867–880; doi: 10.1016/j.cell.2016.07.028
69. Brekk OR, Honey JR, Lee S, et al. Cell type-specific lipid storage changes in Parkinson's disease patient brains are recapitulated by experimental glycolipid disturbance. Proc Natl Acad Sci U S A 2020;117(44):27646–27654; doi: 10.1073/pnas.2003021117
70. Siegrist SE, Haque NS, Chen CH, et al. Inactivation of both Foxo and reaper promotes long-term adult neurogenesis in Drosophila. Curr Biol 2010;20(7):643–648; doi: 10.1016/j.cub.2010.01.060
71. Du S, Jin F, Maneix L, Gedam M, et al. FoxO3 deficiency in cortical astrocytes leads to impaired lipid metabolism and aggravated amyloid pathology. Aging Cell 2021;20(8):e13432; doi: 10.1111/acel.13432
72. Bolukbasi E, Woodling NS, Ivanov DK, et al. Cell type-specific modulation of healthspan by Forkhead family transcription factors in the nervous system. Proc Natl Acad Sci U S A 2021;118(8):e2011491118; doi: 10.1073/pnas.2011491118
73. Davie K, Janssens J, Koldere D, et al. A single-cell transcriptome atlas of the aging drosophila brain. Cell 2018;174(4):982–998 e20; doi: 10.1016/j.cell.2018.05.057
74. Puig O, Tjian R. Transcriptional feedback control of insulin receptor by dFOXO/FOXO1. Genes Dev 2005;19(20):2435–2446; doi: 10.1101/gad.1340505
75. Chandegra B, Tang JLY, Chi H, et al. Sexually dimorphic effects of dietary sugar on lifespan, feeding and starvation resistance in Drosophila. Aging (Albany NY) 2017;4(9):2521–2528; doi: 10.18632/aging.101335
76. Tramunt B, Smati S, Grandgeorge N, et al. Sex differences in metabolic regulation and diabetes susceptibility. Diabetologia 2020;63(3):453–461; doi: 10.1007/s00125-019-05040-3

77. Millington JW, Brownrigg GP, Basner-Collins PJ, et al. Genetic manipulation of insulin/insulin-like growth factor signaling pathway activity has sex-biased effects on *Drosophila* body size. G3 Genes|Genomes|Genetics 2021;11(3):jkaa067; doi: 10.1093/g3journal/jkaa067
78. Vital P, Larrieta E, Hiriart M. Sexual dimorphism in insulin sensitivity and susceptibility to develop diabetes in rats. J Endocrinol 2006;190(2):425–432; doi: 10.1677/joe.1.06596
79. Wilkin TJ, Murphy MJ. The gender insulin hypothesis: Why girls are born lighter than boys, and the implications for insulin resistance. Int J Obes (Lond) 2006;30(7):1056–1061; doi: 10.1038/sj.ijo.0803317
80. Geer EB, Shen W. Gender differences in insulin resistance, body composition, and energy balance. Gend Med 2009;6 Suppl 1:60–75; doi: 10.1016/j.genm.2009.02.002
81. Sepil I, Carazo P, Perry JC, et al. Insulin signalling mediates the response to male-induced harm in female Drosophila melanogaster. Sci Rep 2016;6:30205; doi: 10.1038/srep30205
82. Lakhter AJ, Hamilton J, Konger RL, et al. Glucose-independent acetate metabolism promotes melanoma cell survival and tumor growth. J Biol Chem 2016;291(42):21869–21879; doi: 10.1074/jbc.M115.712166
83. Ma Y, Temkin SM, Hawkridge AM, et al. Fatty acid oxidation: An emerging facet of metabolic transformation in cancer. Cancer Lett 2018;435:92–100; doi: 10.1016/j.canlet.2018.08.006
84. Li H, Feng Z, He M-L. Lipid metabolism alteration contributes to and maintains the properties of cancer stem cells. Theranostics 2020;10(16):7053–7069; doi: 10.7150/thno.41388
85. Gao X, Lin SH, Ren F, et al. Acetate functions as an epigenetic metabolite to promote lipid synthesis under hypoxia. Nat Commun 2016;7:11960; doi: 10.1038/ncomms11960
86. Girard V, Goubard V, Querenet M, et al. Spen modulates lipid droplet content in adult Drosophila glial cells and protects against paraquat toxicity. Sci Rep 2020;10(1):20023; doi: 10.1038/s41598-020-76891-9
87. Goodman LD, Bellen HJ. Recent insights into the role of glia and oxidative stress in Alzheimer's disease gained from Drosophila. Curr Opin Neurobiol 2021;72:32–38; doi: 10.1016/j.conb.2021.07.012
88. Shi L, Shen Y, Min W. Invited Article: Visualizing protein synthesis in mice with in vivo labeling of deuterated amino acids using vibrational imaging. APL Photonics 2018;3(9):092401; doi: 10.1063/1.5028134
89. Zhang L, Shi L, Shen Y, et al. Spectral tracing of deuterium for imaging glucose metabolism. Nat biomed eng 2019;3(5):402–413.
90. Zhang W, Li Y, Fung AA, et al. Multi-molecular hyperspectral PRM-SRS imaging. bioRxiv 2022:2022.07.25.501472; doi: 10.1101/2022.07.25.501472; doi: 10.1038/s41551-019-0393-4
91. Bolte S, Cordelières FP. A guided tour into subcellular colocalization analysis in light microscopy. J Microsc 2006;224(3):213–232; doi: 10.1111/j.1365-2818.2006.01706.x
92. Meijering E. FeatureJ: An ImageJ Plugin Suite for Image Feature Extraction. Available from: https://imagescience.org/meijering/software/featurej/ [Last accessed: January 25, 2021].
93. Wang P, Deng J, Dong J, et al. TDP-43 induces mitochondrial damage and activates the mitochondrial unfolded protein response. PLoS Genet 2019;15(5):e1007947; doi: 10.1371/journal.pgen.1007947

Received: April 22, 2023
Accepted: May 31, 2023
Online Publication Date: June 20, 2023